Dynamic correlation effects in fully differential cross sections for 75-keV proton-impact ionization of helium

Xiaojie Niu, Shiyan Sun,[*] Fujun Wang, and Xiangfu Jia[†]

School of Physics and Information Engineering, Shanxi Normal University, Linfen, Shanxi 041004, People's Republic of China

The effect of final-state dynamic correlation is investigated for helium single ionization by 75-keV proton impact analyzing fully differential cross sections (FDCS). The final state is represented by a continuum correlated wave (CCW-PT) function which accounts for the interaction between the projectile and the residual target ion (PT interaction). This continuum correlated wave function partially includes the correlation of electron-projectile and electron-target relative motion as coupling terms of the wave equation. The transition matrix is evaluated using the CCW-PT function and the Born initial state. The analytical expression of the transition matrix has been obtained. We have shown that this series is strongly convergent and analyzed the contribution of their different terms to the FDCS within the perturbation method. Illustrative computations are performed in the scattering plane and in the perpendicular plane. Both the correlation effects and the PT interaction are checked by the preset calculations. Our results are compared with absolute experimental data as well as other theoretical models. We have shown that the dynamic correlation plays an important role in the single ionization of atoms by proton impact at intermediate projectile energies, especially at large transverse momentum transfer. While overall agreement between theory and the experimental data is encouraging, detailed agreement is lacking. The need for more theoretical and experimental work is emphasized.

I. INTRODUCTION

Correlation is a well-known concept in a wide range of physical processes. Within atomic physics, correlation is a basic ingredient in the description of multielectronic atoms and ions. The effect of correlation has been assumed to be crucial in charged particle collisions with neutral atomic targets and correlation cannot be neglected for the ionization of atoms by electron impact [1–3]. In the case of single ionization by ion impact, correlation can be understood as a lack of internal independence of the components of a system, i.e., the motion of the electron-projectile subsystem is no longer independent of the electron-recoil-ion-target motion. This dynamical coupling between the motion of all particles plays a significant role in all many-body problems (see [4,5] and references therein). One of the simplest systems in which this correlation can be studied is the three-body Coulomb problem. The simplest collision process leading to three free particles in the final state is the ionization of the hydrogen atom by proton impact [6,7]. For nonhydrogenic targets, the ion-atom ionizing collisions can be modeled as a three-body Coulomb problem with appropriate effective charges and offers the opportunity to investigate the full continuum problem. The correlation (or coupling) of the ionized electron moving in the long-range Coulomb potential of two heavy ions directly influences the essence of the dynamical process in the ionization reactions. The details of these states can be revealed by the computation of fully differential cross sections (FDCS) of electronic emission in these collisions.

From a theoretical point of view, the Schrödinger equation for many interacting bodies does not have any known exact analytical solution and some approximations should be consid-ered instead. One of the most successful approaches to describe these three-body states is the well-known 3C wave function, a product of three two-body continuum Coulomb functions representing each of the "independent" interactions between the charged particles [8,9]. In some sense, the 3C function includes a trivial correlation since the relative coordinates and momenta of the particles are linked. Moreover, the 3C state does not introduce any dynamical correlation since the influence of the third particle is neglected at the wave-function level. Other wave functions have been proposed. Many of these proposals are formally similar to the 3C approximation. They introduce correlation through effective Sommerfeld parameters, depending on the coordinates [3] and momenta [1]. A step beyond the 3C model has been introduced by Gasaneo and co-workers (see [10] and references therein) with the use of multivariable hypergeometric functions as approximate solutions to the three-body Schrödinger equation. The wave functions are correlated; that is to say, they are nonseparable solutions of the wave equation which dynamically mix the motion of the electron relative to target and to projectile and verify the Redmond's asymptotic conditions of long-range interactions. It has been denoted the continuum correlated wave (CCW).

The CCW function has been applied to the calculation of the doubly differential cross sections (DDCS) for $H^+ + H$, $H^+ + He$, $C^{6+} + He$, and $F^{9+} + He$ ionizing collisions [5,11,12] under an impact parameter approximation. The success of the theory to reproduce the experimental data has been remarkable. These works have shown that the electron-ion correlation plays an important role in the single ionization of atoms by ion impact in the intermediate- to high-energy regime. However, Ciappina and Cravero [4] have also carried out calculations of the FDCS for the single ionization of helium by 100 MeV/amu C^{6+} projectiles using the same approximation as for the CCW function. They found that the effect of dynamic correlation is very small and does not explain the experimental results. It

is worth noting that the interaction between the projectile and the target ion (PT) is not accounted for in the model. In fact, it has been shown that the PT interaction has a large influence depending on the ejected electron energies and momentum transfer values at intermediate impact energies [6,7,13–16]. It should be necessary to include the PT interaction at the FDCS level. Consequently, the role of the correlation and PT interaction deserves to be analyzed in detail (see [4] and references therein).

In this work, we present the analytic derivation of the FDCS in a Born-like approximation using the CCW function as a final state for the single ionization of a hydrogenlike atom by ion impact. The PT interaction has been accounted for not only in the CCW final state, but in the perturbative potential as well. The initial state is represented as a product of the plane wave for the projectile and the bound-state wave function of a hydrogenlike atom. The purpose of this paper is to explore the role of the correlated effect and the PT interaction in FDCS for intermediate ion impact ionization within the Born-like approximation, and to see if the improvements in the theory represented by the CCW can explain the large discrepancies between experiment and theory which have been found so far. Viewing the success of the CCW model, we are motivated to compare the CCW cross section with the corresponding experimental results as well as other theoretical models, and to assess the ability of the present model to reproduce the peak structure and relative magnitudes of the experimental data.

The organization of the paper is as follows. In Sec. II, the theoretical formalism and evaluation of the transition amplitude are outlined. The obtained results and their related comparisons and discussion are given in Sec. III. Concluding remarks are given in Sec. IV. Atomic units (a.u.) are used unless otherwise stated.

II. THEORETICAL TREATMENTS

We treat helium single ionization as a single-electron process assuming that in the final state, the active target electron moves in the combined Coulomb field of the incoming projectile and the residual-target core with a given effective charge. This charge takes into account the partial screening due to the passive helium electron.

In the center-of-mass (c.m.) frame, the FDCS is given by

$$\frac{d^3\sigma}{d\Omega_P d\Omega_e dE_e} = N_e (2\pi)^4 \mu_{Ie} \mu_{PA}^2 \frac{K_f k_T}{K_i} |T_{fi}|^2. \quad (1)$$

The reduced mass of the helium-ion-electron subsystem is μ_{Ie}, and the reduced mass of the projectile-target atom system is μ_{PA}. The initial and final momenta of the projectile are K_i and K_f, the ejected electron's energy and momentum are given by E_e and k_T, respectively, and N_e is the number of electrons in the atomic shell. The solid angles $d\Omega_P$ and $d\Omega_e$ represent the direction of scattering of the projectile and the ionized electron, respectively.

The main quantity in (1) is the transition matrix T_{fi} in prior form, which can be written as

$$T_{fi} = \langle \Psi_f^- | V_i | \Phi_i^+ \rangle, \quad (2)$$

where the initial-state [final-state] wave function Φ_i^+ [Ψ_f^-] satisfies the outgoing-wave (+) [incoming-wave (−)] boundary conditions and V_i is the initial-channel perturbation.

The undistorted Born initial state reads simply

$$\Phi_i^+(\boldsymbol{r}_T, \boldsymbol{R}_T) = (2\pi)^{-3/2} \exp(\boldsymbol{K}_i \cdot \boldsymbol{R}_T) \Psi_i(\boldsymbol{r}_T). \quad (3)$$

Here, $\boldsymbol{R}_T$ is the position vector of the projectile relative to the atomic center of mass. $\boldsymbol{r}_T$ represents the coordinates of the ionized electron with respect to the target core. The ground state is $\Psi_i(\boldsymbol{r}_T) = (\frac{Z_T^3}{\pi})^{1/2} \exp(-Z_T r_T)$. Z_T is an effective charge given by $Z_T = 1.34$ arising from the binding energy of the active electron that is used. The corresponding initial-channel projectile-atom interaction is

$$V_i = -\frac{Z_P}{r_P} + \frac{Z_P Z_T}{R_T}. \quad (4)$$

Here, $\boldsymbol{r}_P$ is the coordinates of the ionized electron with respect to the projectile and Z_P is the projectile's charge.

The final-state wave function Ψ_f^- (see [10] and references therein) is chosen as

$$\Psi_f^- = N(2\pi)^{-3} \exp(i\boldsymbol{k}_T \cdot \boldsymbol{r}_T + i\boldsymbol{K}_f \cdot \boldsymbol{R}_T) \Phi_2(i\alpha_T, i\alpha_P, 1,$$
$$-ik_T \xi_T, -ik_P \xi_P)_1 F_1(i\alpha_{PT}, 1, -ik_{PT}\xi_{PT}), \quad (5)$$

with

$$N = \exp[-\pi(\alpha_{PT} + \alpha_T + \alpha_P)/2]\Gamma(1 - i\alpha_{PT})$$
$$\times \Gamma(1 - i\alpha_T - i\alpha_P). \quad (6)$$

The function Φ_2 is a two-variable hypergeometric-function solution of a differential equation involving mixed derivatives [10]. However, for evaluation of the transition matrix, it has a more convenient expansion in terms of confluent hypergeometric functions,

$$\Phi_2 = \sum_m a_m (-ik_T \xi_T)^m (-ik_P \xi_P)^m {}_1F_1(i\alpha_T + m, 1$$
$$+ 2m, -ik_T \xi_T)_1 F_1(i\alpha_P + m, 1 + 2m, -ik_P \xi_P), \quad (7)$$

$$a_m = \frac{(-1)^m (i\alpha_T)_m (i\alpha_P)_m}{(m)_m (1)_{2m} m!}, \quad (8)$$

with $(\alpha)_m$ being the Pochammer symbol and $\xi_j = r_j + \hat{k}_j \cdot \boldsymbol{r}_j$ with $j = T, P$, or PT. Here, T, P, and PT represent the target-electron, projectile-electron, and projectile-target interactions, respectively. $\hat{k}_j$ is the unit vector in the direction of the relative momenta $\boldsymbol{k}_j$ for each pair of particles. $\alpha_T = \frac{-Z_T}{k_T}$, $\alpha_P = \frac{-Z_P}{k_P}$, and $\alpha_{PT} = \frac{\mu Z_P Z_T}{k_{PT}}$ represent the $e - T$, $e - P$, and PT Sommerfeld parameter, respectively. μ is the reduced mass of the projectile-target ion subsystem. Equation (7) represents the expansion of a correlated three-body function in terms of a separable set of two-body functions, and each partial sum will give an approximation order. The coupling between the motion of the electron relative to the projectile and the residual ion is approximately introduced by the Φ_2 wave. Hence the dynamically correlated motion of the emitted electron with respect to the heavy ions will be represented by the Φ_2. It has been denoted that the continuum correlated wave (CCW) and the term with $m = 0$ gives the 2C wave [4,5,11,12].

The interaction between the heavy particles is represented by a two-body Coulomb wave function

$_1F_1(i\alpha_{PT};1;-ik_{PT}\xi_{PT})$ in Eq. (5). It is worth noting that besides a normalization factor, the lowest order of this series, i.e., $m = 0$, is the well-known 3C function [8,9]. The internuclear wave function, i.e., PT interaction, can be removed with an impact parameter approximation since they do not contribute to DDCS. However, in the present approximation, the internuclear wave function will be kept not only in the final state, but also in the perturbative potential.

In the heavy mass limit, using the transformation $\boldsymbol{r}_{PT} \approx \boldsymbol{R}_T \equiv \boldsymbol{R}, \boldsymbol{r}_T \equiv \boldsymbol{r}$, and after a large dose of mathematical manipulation that we will not reproduce here, the transition matrix T_{fi} is then given by

$$T_{fi} = \lim_{M\to\infty} T_{fi}^M = \lim_{M\to\infty} C \sum_{m=0}^{M} a_m^* \hat{D} T_m, \tag{9}$$

where

$$\hat{D} = -Z_P \frac{\partial^2}{\partial\varepsilon_1\partial\varepsilon_2} + Z_T Z_P \frac{\partial^2}{\partial\varepsilon_1\partial\varepsilon_3}, \tag{10}$$

$$T_m = \int \frac{d^3r\,d^3R}{rr_pR} \exp(i\boldsymbol{q}\cdot\boldsymbol{R} - ik_T\cdot\boldsymbol{r})\exp[-(\varepsilon_1 + Z_T)r]\exp(-\varepsilon_2 R - \varepsilon_3 r_P)(ik_T r + i\boldsymbol{k}_T\cdot\boldsymbol{r})^m$$
$$\times\,_1F_1(-i\alpha_T + m, 1 + 2m, i(k_T r + \boldsymbol{k}_T\cdot\boldsymbol{r}))(ik_P r_P + i\boldsymbol{k}_P\cdot\boldsymbol{r}_P)^m\,_1F_1(-i\alpha_P + m, 1 + 2m, i(k_P r_P + \boldsymbol{k}_P\cdot\boldsymbol{r}_P))$$
$$\times\,_1F_1(-i\alpha_{PT}, 1, i(k_{PT}R + \boldsymbol{k}_{PT}\cdot\boldsymbol{R})), \tag{11}$$

with $\boldsymbol{q} = \boldsymbol{K}_i - \boldsymbol{K}_f$ (momentum transfer) and $C = N^*(2\pi)^{-3}(2\pi)^{-3/2}(\frac{Z_T^3}{\pi})^{1/2}$. Here we have introduced the parameters $\varepsilon_i(i = 1,2,3)$ for the convenience of our calculations, and take the limit $\varepsilon_i \to 0^+$ after solving the integral.

We note that when $m = 0$, besides a factor, the expression $T_{m=0}$ reduces to the usual 3C approximation in prior form [17,18]. The most important feature of the expression (11) is that the transition matrix can be obtained more generally than Eq. (3) in [19] since the PT interaction modeled by the two-body Coulombic function $_1F_1(-i\alpha_{PT}, 1, i(k_{PT}R + \boldsymbol{k}_{PT}\cdot\boldsymbol{R}))$ is included, whereas it is not included in Eq. (3) in [19]. The six-dimensional integral T_m, which involves three confluent hypergeometric functions, can be analytically reduced to three-dimensional integrals for $m > 0$. It is noteworthy that the second parameter of the two functions $_1F_1(-i\alpha_T + m; 1 + 2m; i(k_T r + \boldsymbol{k}_T\cdot\boldsymbol{r}))$ or $_1F_1(-i\alpha_P + m; 1 + 2m; i(k_P r_P + \boldsymbol{k}_P\cdot\boldsymbol{r}_P))$ is no longer one, but an integer number $1 + 2m$. Therefore, the method used to solve the integral T_0 cannot be directly used to treat the general case $T_{m>0}$. However, we can utilize the derivative formulas of the confluent hypergeometric functions to reduce the integer number $1 + 2m$ to one. For the sake of simplicity, we consider here the derivative representation of the confluent hypergeometric function [20],

$$(ik_T r + i\boldsymbol{k}_T\cdot\boldsymbol{r})^m\,_1F_1(-i\alpha_T + m, 1 + 2m, i(k_T r + \boldsymbol{k}_T\cdot\boldsymbol{r}))$$
$$= \frac{(1 + m)_m}{(-i\alpha_T)_m}\frac{(1)_m}{(-i\alpha_T - m)_m}(ik_T r + i\boldsymbol{k}_T\cdot\boldsymbol{r})^{-m}\frac{\partial^{2m}}{\partial a^{2m}}\,_1F_1(-i\alpha_T - m, 1, ia(k_T r + \boldsymbol{k}_T\cdot\boldsymbol{r}))\,|_{a=1}, \tag{12}$$

$$(ik_P r_P + i\boldsymbol{k}_P\cdot\boldsymbol{r}_P)^m\,_1F_1(-i\alpha_P + m, 1 + 2m, i(k_P r_P + \boldsymbol{k}_P\cdot\boldsymbol{r}_P))$$
$$= \frac{(1 + m)_m}{(-i\alpha_P)_m}\frac{\partial^m}{\partial b^m}\,_1F_1(-i\alpha_P, 1 + m, ib(k_P r_P + \boldsymbol{k}_P\cdot\boldsymbol{r}_P))\,|_{b=1}. \tag{13}$$

Here we have introduced the parameters a and b for the convenience of our calculations, and take the limit $a,b \to 1$ after solving the partial derivative. Inserting Eqs. (12) and (13) into Eq. (11), we can write the scattering amplitude as

$$T_m = \frac{(1 + m)_m}{(-i\alpha_T)_m}\frac{(1)_m}{(-i\alpha_T - m)_m}\frac{(1 + m)_m}{(-i\alpha_P)_m}\frac{\partial^{3m}}{\partial a^{2m}\partial b^m}\int\frac{d^3r\,d^3R}{rr_pR}\exp(i\boldsymbol{q}\cdot\boldsymbol{R} - ik_T\cdot\boldsymbol{r})\exp[-(\varepsilon_1 + Z_T)r]\exp(-\varepsilon_2 R - \varepsilon_3 r_P)$$
$$\times(ik_T r + i\boldsymbol{k}_T\cdot\boldsymbol{r})^{-m}\,_1F_1(-i\alpha_T - m, 1, ia(k_T r + \boldsymbol{k}_T\cdot\boldsymbol{r}))_1F_1(-i\alpha_{PT}, 1, i(k_{PT}R + \boldsymbol{k}_{PT}\cdot\boldsymbol{R}))$$
$$\times\,_1F_1(-i\alpha_P, 1 + m, ib(k_P r_P + \boldsymbol{k}_P\cdot\boldsymbol{r}_P)). \tag{14}$$

To be able to obtain analytical expressions for the transition matrix T_m, we can employ the integral method given in Refs. [17,18]. Therefore, we consider here the integral representation of the confluent hypergeometric functions [20] in Eq. (14),

$$_1F_1(a, 1, z) = \frac{1}{2\pi i}\oint_{C_i} dt_i\, t_i^{a-1}(t_i - 1)^{-a}\exp(zt_i), \tag{15}$$

for the first two confluent hypergeometric functions, and the last one,

$$_1F_1(-i\alpha_P, 1 + m, ib(k_P r_P + \boldsymbol{k}_P\cdot\boldsymbol{r}_P)) = \frac{\Gamma(1 + m)}{\Gamma(-i\alpha_P)\Gamma(1 + m + i\alpha_P)}\int_0^1 dt\, t^{-i\alpha_P-1}(1 - t)^{i\alpha_P+m}\exp[ibt(k_P r_P + \boldsymbol{k}_P\cdot\boldsymbol{r}_P)]. \tag{16}$$

And the negative power function in Eq. (14) is written as

$$(ik_T r + i\boldsymbol{k}_T \cdot \boldsymbol{r})^{-m} = \begin{cases} \frac{i^{-m}}{\Gamma(m)} \int_0^\infty \tau^{m-1} e^{-\tau(k_T r + \boldsymbol{k}_T \cdot \boldsymbol{r})} d\tau, & m \geqslant 1 \\ 1, & m = 0. \end{cases} \tag{17}$$

The contour C_i in Eq. (15) is closed and encircles, in the positive direction, the two branch point singularities at $t = 0$ and $t = 1$. Making use of Eqs. (15)–(17) and performing some manipulations, we have

$$T_m = \frac{(1+m)_m}{(-i\alpha_T)_m} \frac{(1)_m}{(-i\alpha_T - m)_m} \frac{(1+m)_m}{(-i\alpha_P)_m} \frac{\partial^{3m}}{\partial a^{2m} \partial b^m} \frac{\Gamma(1+m)}{\Gamma(-i\alpha_P)\Gamma(1+m+i\alpha_P)} \int_0^1 dt\, t^{-i\alpha_P - 1}(1-t)^{i\alpha_P + m} \frac{i^{-m}}{\Gamma(m)} \int_0^\infty d\tau\, \tau^{m-1}$$

$$\times \frac{1}{(2\pi i)^2} \oint_{C_1} \oint_{C_2} dt_1 dt_2 t_1^{-i\alpha_{PT} - 1}(t_1 - 1)^{i\alpha_{PT}} t_2^{-i\alpha_T - m - 1}(t_2 - 1)^{i\alpha_T + m} J_m, \tag{18}$$

with

$$J_m = \int \frac{d^3 r\, d^3 R}{r\, r_P\, R} \exp(-i\boldsymbol{p}_1 \cdot \boldsymbol{r} + i\boldsymbol{p}_2 \cdot \boldsymbol{R} - \xi_1 r - \xi_2 R - \xi_3 r_P), \tag{19}$$

where

$$\boldsymbol{p}_1 = \beta \boldsymbol{q} + \boldsymbol{k}_T - i\tau \boldsymbol{k}_T - bt\boldsymbol{k}_P - at_2 \boldsymbol{k}_T, \quad \boldsymbol{p}_2 = \boldsymbol{q} - bt\boldsymbol{k}_P + t_1 \boldsymbol{k}_{PT},$$

$$\xi_1 = Z_T + \varepsilon_1 + \tau k_T - iat_2 k_T, \quad \xi_2 = \varepsilon_2 - it_1 k_{PT}, \xi_3 = \varepsilon_3 - ibt k_P. \tag{20}$$

The space integration J_m of Eq. (19) can be evaluated by using Fourier transform techniques and following Lewis [21]. Now, for the convenience of later integrations with respect to t_1 and t_2, we express, following Sinha and Sil [22], the results obtained after space integration as

$$J_m = (4\pi)^2 \int_0^\infty ds(\alpha s^2 + 2\beta s + \gamma)^{-1}, \tag{21}$$

where

$$\alpha = [(\boldsymbol{p}_1 - \boldsymbol{p}_2)^2 + (\xi_1 + \xi_2)^2], \quad \gamma = [(\xi_1 + \xi_3)^2 + \boldsymbol{p}_1^2][(\xi_2 + \xi_3)^2 + \boldsymbol{p}_2^2],$$

$$\beta = \xi_1(\xi_3^2 + \boldsymbol{p}_2^2 + \xi_2^2) + \xi_2(\xi_3^2 + \boldsymbol{p}_1^2 + \xi_1^2) + \xi_3[(\boldsymbol{p}_1 - \boldsymbol{p}_2)^2 + (\xi_1^2 + \xi_2^2)]. \tag{22}$$

The expressions for α, β, and γ are linear functions of t_1 and/or t_2. Thus we can write $\alpha s^2 + 2\beta s + \gamma$ as $\sigma_0 + \sigma_1 t_1 + \sigma_2 t_2 + \sigma_{12} t_1 t_2$, where σ_0, σ_1, σ_2, and σ_{12} are the functions of s and t. Hence, Eq. (21) can be recast into the following form:

$$J_m = (4\pi)^2 \int_0^\infty ds(\sigma_0 + \sigma_1 t_1 + \sigma_2 t_2 + \sigma_{12} t_1 t_2)^{-1}. \tag{23}$$

Thus, we have

$$T_m = (4\pi)^2 \frac{(1+m)_m}{(-i\alpha_T)_m} \frac{(1)_m}{(-i\alpha_T - m)_m} \frac{(1+m)_m}{(-i\alpha_P)_m} \frac{\Gamma(1+m)}{\Gamma(-i\alpha_P)\Gamma(1+m+i\alpha_P)}$$

$$\times \int_0^1 dt\, t^{-i\alpha_P - 1}(1-t)^{i\alpha_P + m} \frac{i^{-m}}{\Gamma(m)} \int_0^\infty d\tau\, \tau^{m-1} \int_0^\infty ds \frac{\partial^{3m}}{\partial a^{2m} \partial b^m} I_c, \tag{24}$$

where

$$I_c = \frac{1}{(2\pi i)^2} \oint_{C_1} \oint_{C_2} \frac{dt_1 dt_2 t_1^{-i\alpha_{PT} - 1}(t_1 - 1)^{i\alpha_{PT}} t_2^{-i\alpha_T - m - 1}(t_2 - 1)^{i\alpha_T + m}}{\sigma_0 + \sigma_1 t_1 + \sigma_2 t_2 + \sigma_{12} t_1 t_2}. \tag{25}$$

Hence, Eq. (25) can be integrated by the residue theorem, which has been discussed in detail in Refs. [17,18], and we obtain

$$I_c = \frac{1}{\sigma_0} \left(\frac{\sigma_0}{\sigma_0 + \sigma_1}\right)^{-i\alpha_{PT}} \left(\frac{\sigma_0}{\sigma_0 + \sigma_2}\right)^{-i\alpha_T - m} {}_2F_1\left[-i\alpha_{PT}, -i\alpha_T - m; 1; \frac{\sigma_1 \sigma_2 - \sigma_0 \sigma_{12}}{(\sigma_0 + \sigma_1)(\sigma_0 + \sigma_2)}\right], \tag{26}$$

where ${}_2F_1$ is Gauss-hypergeometric function.

Finally, we have Eq. (24) as

$$
T_m = (4\pi)^2 \frac{(1+m)_m}{(-i\alpha_T)_m} \frac{(1)_m}{(-i\alpha_T - m)_m} \frac{(1+m)_m}{(-i\alpha_P)_m} \frac{\Gamma(1+m)}{\Gamma(-i\alpha_P)\Gamma(1+m+i\alpha_P)} \int_0^1 dt\, t^{-i\alpha_P-1}(1-t)^{i\alpha_P+m} \frac{i^{-m}}{\Gamma(m)} \int_0^\infty d\tau\, \tau^{m-1}
$$

$$
\times \int_0^\infty ds \frac{\partial^{3m}}{\partial a^{2m}\partial b^m} \left[\frac{1}{\sigma_0} \left(\frac{\sigma_0}{\sigma_0+\sigma_1} \right)^{-i\alpha_{PT}} \left(\frac{\sigma_0}{\sigma_0+\sigma_2} \right)^{-i\alpha_T-m} {}_2F_1\left(-i\alpha_{PT}, -i\alpha_T - m; 1; \frac{\sigma_1\sigma_2 - \sigma_0\sigma_{12}}{(\sigma_0+\sigma_1)(\sigma_0+\sigma_2)} \right) \right]. \quad (27)
$$

We should bear in mind here $m > 0$ in Eq. (27). In order to check our results, we note Eq. (17), and after taking $m = 0$ and this moment $\tau = 0$, we have

$$
T_0 = (4\pi)^2 \frac{\Gamma(1)}{\Gamma(-i\alpha_P)\Gamma(1+i\alpha_P)} \int_0^1 dt\, t^{-i\alpha_P-1}(1-t)^{i\alpha_P} \int_0^\infty ds \frac{1}{\sigma_0} \left(\frac{\sigma_0}{\sigma_0+\sigma_1} \right)^{-i\alpha_{PT}} \left(\frac{\sigma_0}{\sigma_0+\sigma_2} \right)^{-i\alpha_T}
$$

$$
\times {}_2F_1\left(-i\alpha_{PT}, -i\alpha_T; 1; \frac{\sigma_1\sigma_2 - \sigma_0\sigma_{12}}{(\sigma_0+\sigma_1)(\sigma_0+\sigma_2)} \right). \quad (28)
$$

Equation (28), apart from a factor, is the commonly known 3C approximation in prior form [9,17,18,23]. Therefore, a three-dimensional integral is reached with $m > 0$ and can be evaluated numerically to calculate T_m. The final state given by Eq. (7) leads to an infinite expansion of the transition amplitude T_{fi} [see Eq. (9)], which has fast convergence, and for practical calculations the sum of only a few terms of that expansion is enough to obtain a stable value for the whole transition amplitude.

We observe that this formula (27) is different from the ones given by Eqs. (22), (25), and (28) in [19]. Here, Eq. (27) can be considered as an extended integral form of Eq. (3) in Ref. [19] based on the CCW function (5). The analytical expression of the 3mth order partial derivatives of these composite functions in Eq. (27) can be carried out by the MATHEMATICA package. In addition, the parameters of ε_1, ε_2, and ε_3 are introduced for convenience in the present calculations, and attention should be paid to the derivation of ε_1, ε_2, and ε_3. In the derivation of each variable, a forward-difference formula is utilized to keep the variable positive when it approaches zero. These integrals have been performed numerically by the Gauss-Legendre quadrature method. Convergence of the results has been tested by increasing the number of quadrature points to achieve an accuracy of 0.1%. Furthermore, we label the present calculation using the above wave function (5), perturbation potential (4), and transition matrix (9) as CCW-PT to distinguish it from the usual CCW [4,5,11,12,19] theory where the PT interaction is not accounted for (hereafter referred to as the CCW-noPT). The CCW-noPT calculation can be obtained by setting $\alpha_{PT} = 0$ in (5) or (27) and (28), and the well-known 2C approximation can be recovered by setting $\alpha_{PT} = 0$ and $M = 0$.

III. RESULTS AND DISCUSSION

In order to check the accuracy of the present model, we have computed the FDCS, by Eq. (1), for 75-keV proton-impact ionization of helium and electron ejected into both the scattering plane (Fig. 1) and the perpendicular plane (Fig. 2) with $E_e = 5.4$ eV, which corresponds to the experimental data of [24]. Here we have modeled the final interaction with the target by an effective charge $Z_T = 1.34$ that leads to the correct energy of the bound state. We should point out that this

is a very approximate way to include the effect of the passive electron of helium in the final state.

As mentioned above, the series expansion in the transition matrix has an excellent numerical convergence, and we have computed the individual FDCS by setting $m = 0, 1, \ldots, 5$ in the scattering amplitude T_m, respectively. We find that the contribution to the FDCS is mainly from the first three terms of the series. The higher terms ($m > 3$) are several orders of magnitude smaller than the first one. The convergence is also shown in Figs. 1(a) and 2(a), where the FDCS calculated with $M = 0, \ldots, 5$, i.e., the individual FDCS for $m = 0, 1, \ldots, 5$, have been summed, where each result represents the coherent sum of different orders in the transition matrix. It is worth noting that the calculations using $m = 0$ or $M = 0$ are the lowest order in the transition matrix; the expression (9) reduces to the 3C approximation. As seen from Figs. 1(a) and 2(a), besides the CCW-PT ($M = 0-2$), the shape and the magnitudes of each theoretical curve are approximately the same, respectively. That is to say, the $m = 0, \ldots, 3$ FDCS are the dominant contribution to the sum. This is further confirmation that considering up to order $M = 3$ is enough to calculate the FDCS in the CCW-PT approximation.

In Fig. 1, we show the angular distribution of the FDCS for electrons with an energy of 5.4 eV ejected into the scattering plane. To study the effects of final-state correlation, we compare the theoretical values given by the CCW-PT, 3C calculations, and the three-body distorted wave (3DW) approximations [24] with the experimental data of Schulz et al. [24]. The theoretical results multiplied by a proper factor are compared to the experiment data. Consequently, we can take a qualitative look at the differences among these theoretical results. Both the theoretical curves and experimental results showed the binary peak approximately in the direction of $\boldsymbol{q}$. In the experiment, the binary peak is shifted in the backward direction relative to $\boldsymbol{q}$ at small q_t, and, eventually turns into a forward shift at large q_t. It can be seen from Fig. 1 that the qualitative agreement between the binary peak observed in the CCW-PT results and in the experiment is satisfactory except for some small shifts. Most noticeably, the angular distributions and relative magnitude differences are found between the CCW-PT and 3C results (the two calculations are multiplied by the same factors) in this region. We would like to explain that these differences are
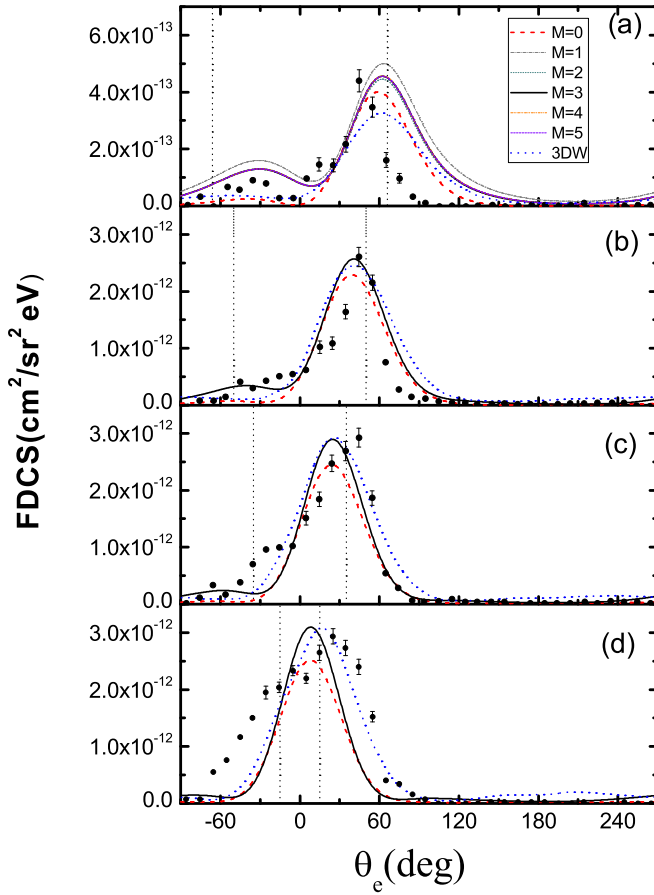
FIG. 1. Fully differential cross sections for electrons with an energy that is 5.4 eV ejected into the scattering plane in 75-keV $p +$ He collisions. The present FDCS have been plotted against the angle of the ejected electron (θ_e). The dotted vertical line at positive angles denotes the angle θ_q of q relative to K_i, and the ones at negative angles indicate $-\theta_q$. The transverse momentum transfers q_t are (a) $q_t = 1.38$, (b) $q_t = 0.73$, (c) $q_t = 0.41$, and (d) $q_t = 0.13$ a.u. The 3C (dashed red lines) and CCW-PT (solid black lines) calculations multiplied by 0.5 (0.73 a.u.), 0.22 (0.41 a.u.), and 0.14 (0.13 a.u.), respectively. Dotted blue lines: 3DW calculations [24] multiplied by 0.6 (0.73 a.u.), 0.3 (0.41 a.u.), and 0.2 (0.13 a.u.), respectively. Solid circles are for experimental measurements [24].

due to the CCW-PT approximations in which the correlation is considered.

Due to a two-step scattering mechanism, a smaller peak is called the recoil peak, which is usually seen approximately in the opposite of q. However, no recoil peak in the direction of $-q$ was observed experimentally. On the contrary, a strong peak structure near $-\theta_q$ was found; the structure was attributed to the recoil peak being strongly shifted in the forward direction [24,25] and the peak becomes more visible with increasing q_t. For this peak structure, remarkable discrepancies are observed between the correlated (CCW-PT) and the uncorrelated (3C) wave-function calculations, particularly in the case of $q_t = 0.41, 0.73$ and 1.38 a.u. In Fig. 1, we can see that the 3C results show the peak in the expected angular region for larger q_t, but the experimental data is seriously underestimated; as a result, the peak structure is less pronounced than the experiment. Furthermore, the peak structure is nearly absent for smaller
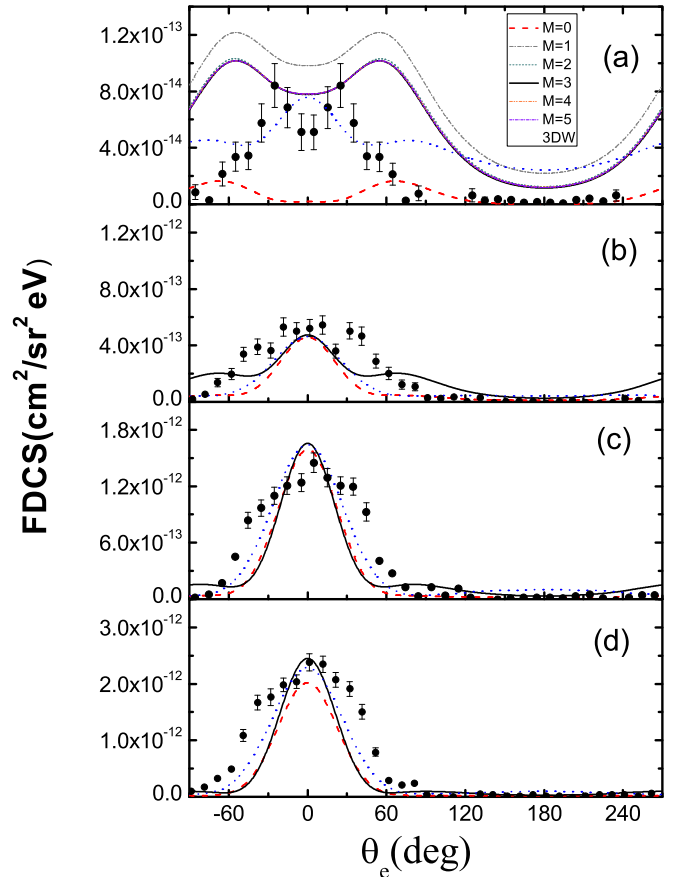
FIG. 2. The notation is the same as in Fig. 1 but for the electron emission into the perpendicular plane. The 3C (dashed red lines) and CCW-PT (solid black lines) calculations multiplied by 0.52 (0.73 a.u.), 0.26 (0.41 a.u.), and 0.12 (0.13 a.u.), respectively. Dotted blue lines: 3DW calculations [24] multiplied by 3 (1.38 a.u.), 0.6 (0.73 a.u.), 0.3 (0.41 a.u.), and 0.2 (0.13 a.u.), respectively. Solid circles are for experimental measurements [24].

q_t. It is clear that the inclusion of correlation in the CCW-PT calculations leads to a very distinct recoil peak, whereas the peak is completely absent in the 3DW calculations for all q_t. We can conclude that the peak structure is provided by the lowest order ($m = 0$), and higher orders are responsible for the enhancement of the structure. Additionally, in the absolute magnitude, much better agreement is achieved with our CCW-PT calculation for the largest q_t in the scattering plane. Here, the inclusion of correlation does seem to introduce a relevant advantage in the description of the scattering plane and should not be neglected.

The 3C and CCW-PT calculations and the 3DW results are also plotted in Fig. 2. The experimental FDCS exhibit a strong peak at $\theta_e = 0°$ except for $q_t = 1.38$ a.u. It has been observed that this maximum becomes broader with increasing q_t, and eventually separates into two peaks at about $\theta_e = \pm 30°$ for the largest q_t, leaving a minimum at $\theta_e = 0°$. That is to say, signatures of the higher-order contributions tend to increase in the perpendicular plane [24]. In fact, the two-peak structure has been observed at about $\theta_e = \pm 40°$ in the case of $q_t = 0.73$ a.u. experimentally. In Fig. 2(b), the experimental FDCS is well described by CCW-PT, since the CCW-PT predicts two maxima

at about $\theta_e = \pm 65°$ and the two peaks are not found in the 3C and 3DW results. The CCW-PT and 3C calculations reproduce the position of the maximum at $\theta_e = 0°$ except for the largest q_t. For the largest q_t, the two peaks occur at about $\theta_e = \pm 70°$, and the minimum at $\theta_e = 0°$ shows virtually zero cross section for the 3C calculation, while, taking the higher terms ($m > 0$) into account, the two peaks occur at $\theta_e = \pm 55°$ for CCW-PT. At the same time, the overall magnitude of the FDCS is improved significantly. We should note that the CCW-PT exaggerates the FDCS for $q_t = 1.38$ a.u. by as much as an order of magnitude as compared to the 3C results. In other words, the features observed in the measured FDCS are still provided by the lowest order, allowing the electron to interact with the target ion, and the projectile to higher orders in the final state improves the agreement between experiment and theory. We can now turn our attention to the 3DW calculations, although the 3DW calculations seem to reproduce the position of the maximum fairly well for the smaller q_t. In the case of $q_t = 1.38$ a.u., it is in poor agreement with the measurements in shape and magnitude, and the minimum is absent for the 3DW model. In contrast, there exists a maximum at $\theta_e = 0°$. Furthermore, the 3DW results have the two-peak structure at about $\theta_e = \pm 80°$; nevertheless, the two peaks that are seen from the experimental data are at about $\theta_e = \pm 30°$. The failure of the 3DW model predicting the two peaks might have been traced back to the absence of the correlated final state. Overall, the CCW-PT model for this description is more suitable than 3DW and 3C.

In order to evaluate the contributions of the correlation effects and the PT interaction, we have also performed calculations using the 2C ($M = 0$, $\alpha_{PT} = 0$) and the CCW-noPT ($\alpha_{PT} = 0$) models. We start here with the 2C, successively adding the correlation and the PT interaction using the respective method of these models. The data of Fig. 1 are shown again in Fig. 3, but this time they are compared to different theoretical curves. The dotted and the dashed lines represent the 2C and the CCW-noPT calculations, respectively. The solid curves still represent the CCW-PT results. According to Fig. 3, the 2C calculations generally describe the trend of the experimental data correctly. However, the 2C results overestimate both the magnitude and the width of the binary peak (as it clearly does at large q_t). At the same time, there is an increasing backward shift with increasing q_t for the binary peak. Only after the correlation is included (CCW-noPT) is a pronounced narrowing compared to the 2C observed for the binary peak, and the magnitude of the binary peak is reduced. However, the inclusion of correlation leads to a distinct recoil peak. Somewhat unexpectedly, with increasing q_t, the magnitude and width of the recoil peak is increasingly overestimated by the CCW-noPT calculation. In contrast to this, the experimental data show a slight recoil peak for all q_t. The intensity of the recoil peak is even larger than the binary one, particularly in the case of $q_t = 0.73$ and 1.38 a.u. This feature of the recoil peak may be qualitatively explained by strong correlation from the CCW function. After the PT interaction is switched on, dramatic improvement of the FDCS as compared with the corresponding distributions in Fig. 3 can be observed by CCW-PT. In spite of the CCW-PT calculations not being completely satisfactory in reproducing the experimental data, the relative success is obtained in the description of the overall features of FDCS and gives results that are closer to the exper-
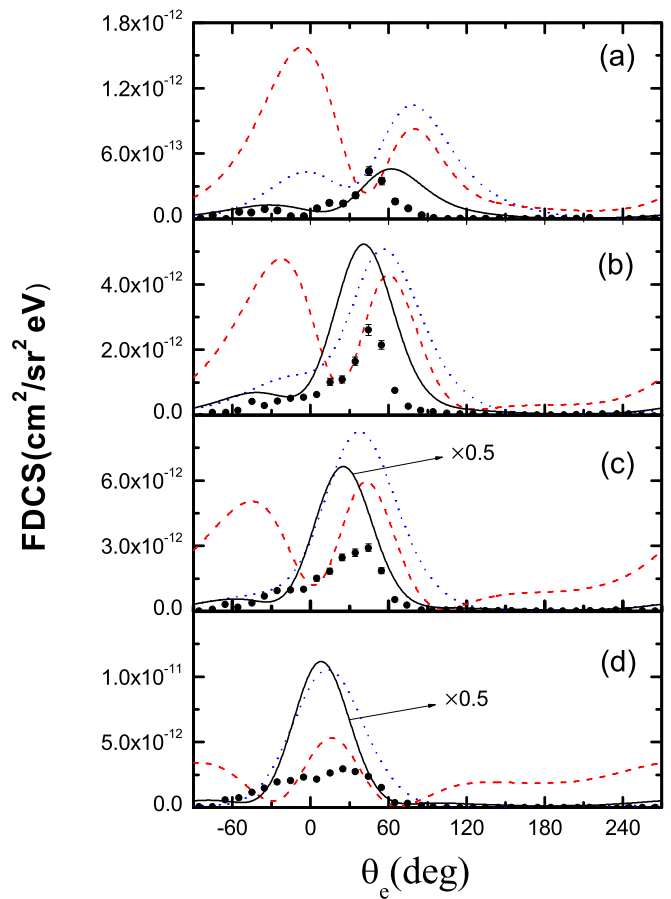
FIG. 3. Same as Fig. 1, but calculations are 2C: dotted blue curves; CCW-noPT: dashed red curves; and CCW-PT: solid black curves.

imental measurement. Furthermore, much better agreement in magnitude is obtained with the CCW-PT calculation at large $q_t = 1.38$ a.u. This confirms that both the correlation and the PT interaction, which are simultaneously accounted for in CCW-PT, can take a relatively important role in the description of this collision process, especially at large q_t. Under these circumstances, the 2C results can be significantly improved.

As mentioned above, signatures of the correlation and PT interaction are observed in the scattering plane. Such effects should be even more pronounced in the perpendicular plane [13]. In Fig. 4, except for the largest q_t, the 2C reproduces the shape of the maximum at $\theta_e = 0°$ and the width of the peak fairly well. Furthermore, there is significant disagreement in magnitude. It is important to note that the 2C does not even remotely resemble the experimental data at $q_t = 1.38$ a.u. It predicts a second pronounced peak at $\theta_e = 180°$, which is not present at all in the data. Some improved agreement with the data is achieved with the CCW-noPT calculation to the extent that the peak at $\theta_e = 180°$ for $q_t = 1.38$ a.u. is completely absent. On the other hand, there is no improved agreement in the absolute magnitude and, in fact, particularly at large q_t the discrepancy is even much larger than for the 2C. Most noticeable is the peaklike character appearing in the CCW-noPT at about $\theta_e = \pm 90°$ in Figs. 4(c) and 4(d), as no such peak is found by the 2C calculations. Besides, the CCW-noPT results overestimate the FDCS in the angular
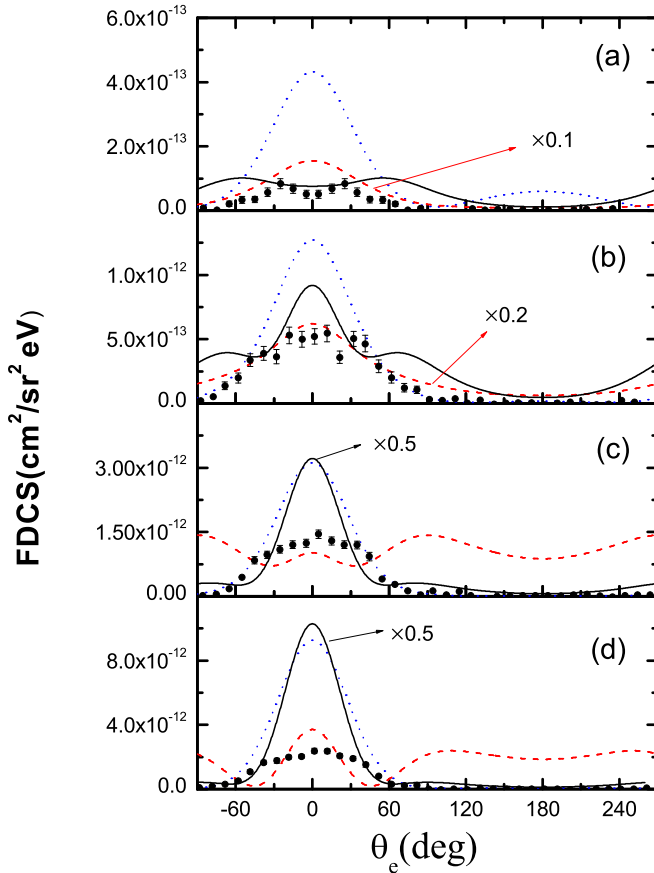
FIG. 4. Same as in Fig. 3, but for electron ejected into the perpendicular plane.

region between $\theta_e = 120°$ and $\theta_e = 270°$ at small q_t. It should again be noted that differences between the 2C and CCW-noPT are some signatures of the correlation. In spite of significant improvement with the data achieved with the CCW-PT calculation, many discrepancies remain. On one hand, the two peaks for small q_t are reduced to a small residue. Furthermore, peak structures are now seen at larger q_t and the calculation is capable of predicting a minimum at $\theta_e = 0°$ in the case of $q_t = 1.38$ a.u. On the other hand, those maxima occur at about $\theta_e = \pm 55°$, nevertheless, the data structure is at about $\theta_e = \pm 30°$. Perhaps the most remarkable aspect of the CCW-PT results is that they reproduce, apart from possibly overestimating the overall magnitude, the measured FDCS for $q_t = 1.38$ a.u. fairly well, in sharp contrast to other theoretical calculations. Finally, the comparison among these calculations shows that the present results are in close proximity with the experimental findings. It also indicates that the correlation and PT interaction should be considered overall to generate such structure, especially at large q_t.

IV. CONCLUSIONS AND PERSPECTIVES

In this work, we have calculated FDCS for the single ionizing of helium by a 75-keV proton impact. We used the CCW function introduced [10] as the final three-body state. We obtained analytical expressions of the transition matrix for the perturbative approximation through a series representation of the CCW function. For the transition matrix,

the PT interaction has been included not only in the final state, but in the perturbative potential. We have assessed the correlation taken into account in CCW-PT theory comparing it with the usual 3C and 3DW calculations. We found that the 3C and CCW-PT calculations have the similar behavior at small q_t. The CCW-PT model is overall in good agreement at large q_t, but not perfect agreement with the measured data. It also shows that the final-state dynamic correlation becomes stronger with increasing q_t. A feature that the correlation described by CCW-PT gives rises to is the enhancement presented by the FDCS. The data were compared to other theoretical calculations and the large differences between the various models show that the cross sections are quite sensitive to the details of the description of the PT interaction. For example, if only the correlated effect is accounted for (CCW-noPT), the calculated FDCS bears no resemblance to the experimental data at all in some aspects, and somewhat worse than the 2C. On the other hand, if the PT interaction is incorporated on top of the correlation, reasonable qualitative agreement is achieved. It may also be noted that with the increase of q_t, the PT interaction becomes more prominent. It is conceivable that the features observed in the data are not only due to the correlation, but to a large extent due to the PT interaction. This was consistent with the large body of already published papers on single ionization [6,7,13–16,24].

The CCW-PT model combines the favored methods of including the correlation and PT interaction and as a result yields the best overall agreement with experiment among the models presented here. However, the description of CCW-PT is still incomplete and it is necessary to include some improvements to the distorted-wave-type theories. For example, the effect of the non-Coulomb part of the interaction between the ejected electron and the residual-target ion should be incorporated, e.g., by using the model potential; a correlated initial channel should be considered instead of the simple Born initial one, e.g., the application of this method in Ref. [12]; and a full four-body approach in which the passive electron fully participates in the collision should be investigated.

To avoid the complications introduced by a many-electron target for an effective three-body problem, $p + $ H (pure three-body system) represents the simplest system for which ionization can occur and theory is not plagued by having to deal with a complicated many-electron state. In fact, it is an ideal system in which to study correlation. The role of the dynamic correlation and PT interaction has also been found to be critical when we applied the present CCW-PT model to deal with the pure three-body problem at the FDCS level. Unfortunately, for proton-impact ionization of atomic hydrogen, fully differential measurements are not available, but there are double-differential measurements from [6,7]. Therefore, it allows us to apply our CCW-PT theory to the basic collision of hydrogen ionization by proton and the measurements are suited to test the theoretical description of the correlation. Our efforts are currently underway.

[1] J. Berakdar and J. S. Briggs, Phys. Rev. Lett. **72**, 3799 (1994).

[2] J. Berakdar, J. S. Briggs, and H. Klar, J. Phys. B **26**, 285 (1993).

[3] J. Berakdar, Phys. Rev. A **53**, 2314 (1996).

[4] M. F. Ciappina and W. R. Cravero, Nucl. Instr. and Methods Phys. Res. B **266**, 555 (2008).

[5] F. D. Colavecchia, G. Gasaneo, and C. R. Garibotti, J. Phys. B **33**, L467 (2000).

[6] A. C. Laforge, K. N. Egodapitiya, J. S. Alexander, A. Hasan, M. F. Ciappina, M. A. Khakoo, and M. Schulz, Phys. Rev. Lett. **103**, 053201 (2009).

[7] M. Schulz, A. C. Laforge, K. N. Egodapitiya, J. S. Alexander, A. Hasan, M. F. Ciappina, A. C. Roy, R. Dey, A. Samolov, and A. L. Godunov, Phys. Rev. A **81**, 052705 (2010).

[8] C. R. Garibotti and J. E. Miraglia, Phys. Rev. A **21**, 572 (1980).

[9] M. Brauner, J. S. Briggs, and H. Klar, J. Phys. B: At. Mol. Opt. Phys. **22**, 2265 (1989).

[10] G. Gasaneo, F. D. Colavecchia, C. R. Garibotti, J. E. Miraglia, and P. Macri, Phys. Rev. A **55**, 2809 (1997).

[11] F. D. Colavecchia, G. Gasaneo, and C. R. Garibotti, Phys. Rev. A **58**, 2926 (1998).

[12] M. F. Ciappina, S. Otranto, and C. R. Garibotti, Phys. Rev. A **66**, 052711 (2002).

[13] M. F. Ciappina, W. R. Cravero, and M. Schulz, J. Phys. B: At. Mol. Opt. Phys. **40**, 2577 (2007).

[14] M. F. Ciappina and W. R. Cravero, J. Phys. B: At. Mol. Opt. Phys. **39**, 2183 (2006).

[15] L. Sarkadi, Phys. Rev. A **82**, 052710 (2010).

[16] Y. H. Duan, S. Y. Sun, and X. F. Jia, Europhys. Lett. **110**, 13001 (2015).

[17] X. F. Jia, Q. C. Shi, Z. J. Chen, J. Chen, and K. Z. Xu, Phys. Rev. A **55**, 1971 (1997).

[18] A. Bandyopadhyayt, K. Roy, P. Mandal, and N. C. Sil, J. Phys. B **27**, 4337 (1994).

[19] F. D. Colavecchia, G. Gasaneo, and C. R. Garibotti, J. Math. Phys. **38**, 6603 (1997).

[20] I. S. Gradsheteyn and I. M. Byzhik, *Tables of Integrals, Series, and Products* (Academic, New York, 2007).

[21] R. R. Lewis, Phys. Rev. **102**, 537 (1956).

[22] C. Sinha and N. C. Si1, J. Phys. B **11**, L333 (1978).

[23] X. Y. Ma, X. Li, S. Y. Sun, and X. F. Jia, Europhys. Lett. **98**, 53001 (2012).

[24] M. Schulz, A. Hasan, N. V. Maydanyuk, M. Foster, B. Tooke, and D. H. Madison, Phys. Rev. A **73**, 062704 (2006).

[25] M. Schulz, R. Moshammer, A. N. Perumal, and J. Ullrich, J. Phys. B **35**, L161 (2002).